PCCP

PAPER

View Article Online
View Journal | View Issue

Open Access Article. Published on 13 September 2023. Downloaded on 3/3/2026 10:42:57 PM.
This article is licensed under a Creative Commons Attribution-NonCommercial 3.0 Unported Licence.

Check for updates

Cite this: *Phys. Chem. Chem. Phys.*, 2023, **25**, 26779

A local point of view of the Cu(100) → NiTPP charge transfer at the NiTPP/Cu(100) interface†

Silvia Carlotto,[ab] Alberto Verdini,*[c] Giovanni Zamborlini,[d] Iulia Cojocariu,[ef] Vitaliy Feyer,[gh] Luca Floreano[i] and Maurizio Casarin*[a]

Received 22nd August 2023,
Accepted 13th September 2023

DOI: 10.1039/d3cp04021f

rsc.li/pccp

A precise understanding, at the molecular level, of the massive substrate → adsorbate charge transfer at the NiTPP/Cu(100) interface has been gained through the application of elementary symmetry arguments to the structural determination of the NiTPP adsorption site by photoelectron diffraction (PED) measurements and Amsterdam density functional calculations of the free D_{4h} NiTPP electronic structure. In particular, the PED analysis precisely determines that, among the diverse NiTPP chemisorption sites herein considered (fourfold hollow, atop, and bridge), the fourfold hollow one is the most favorable, with the Ni atom located at 1.93 Å from the surface and at an internuclear distance of 2.66 Å from the nearest-neighbors of the substrate. The use of elementary symmetry considerations enabled us to provide a convincing modeling of the NiTPP–Cu(100) anchoring configuration and an atomistic view of the previously revealed interfacial charge transfer through the unambiguous identification of the adsorbate π* and σ* low-lying virtual orbitals, of the substrate surface atoms, and of the linear combinations of the Cu 4s atomic orbitals involved in the substrate → adsorbate charge transfer. In addition, the same considerations revealed that the experimentally reported Ni(II) → Ni(I) reduction at the interface corresponds to the fingerprint of the chemisorption site of the NiTPP on Cu(100).

Introduction

The incipit of Ghosh's contribution to the collective volume Letters to a Young Chemist is worded as follows: "Porphyrins are everywhere, as far as the living world is concerned".[1] Although detectable in abiotic systems, the pivotal role played by porphyrin-related molecules in fundamental biological processes such as oxygen transport and storage (haemoglobin and myoglobin), photosynthesis (chlorophyll), and electron transport during cellular respiration and photosynthesis (cytochromes)[2,3] supports their evocative classification: "pigments of life".[4,5] Additionally, porphyrin derivatives have been extensively used in cancer treatment due to their therapeutic and diagnostic properties.[6] Besides the living world, the relevance of this class of molecules extends nowadays to technological fields ranging from electronics,[7] to solar cells,[8] and sensors,[9] thus justifying the constantly rising interest towards them and motivation to develop new porphyrin-like species, whose electronic and optical properties can be tuned through molecular engineering.[10–13] Therefore, surface-supported supramolecular porphyrin arrays may be thought of as functional components in nanodevices.[14] In addition, adsorbate–substrate and adsorbate–adsorbate interactions often lead to charge transfer between the adsorbate frontier molecular orbitals (MO)[15] and the substrate,[16,17] resulting in the addition of spin freedom degrees,[18,19] when using magnetic substrates, through the generation of spin-polarized hybrid interface states.[20,21] The electronic and magnetic properties of surface-supported metal (M) porphyrin arrays can be further customized through the coordination of axial ligands to M,[19,22–25] which can modify the M oxidation number, its spin state, and then its magnetic moment, thus affecting the magnetic anisotropy. Indeed, small molecules such as NO, NH_3, and NO_2 have been shown to bind to the central M of porphyrins, inducing changes in its spin state. The bonding with the surface

[a] University of Padova, Department of Chemical Sciences, via F. Marzolo 1, 35131, Padova, Italy. E-mail: maurizio.casarin@unipd.it
[b] ICMATE - CNR c/o University of Padova, Department of Chemical Sciences, via F. Marzolo 1, via F. Marzolo 1, 35131, Padova, Italy
[c] IOM – CNR c/o University of Perugia, Department of Physics and Geology, via A. Pascoli, 06123, Perugia, Italy
[d] TU Dortmund University, Department of Physics, Otto-Hahn-Straβe 4, 44227 Dortmund, Germany
[e] University of Trieste, Department of Physics, Via A. Valerio 2, 34127 Trieste, Italy
[f] Elettra-Sincrotrone, S.C.p.A., S.S. 14 - km 163.5, 34149 Trieste, Italy
[g] Forschungszentrum Jülich GmbH, Peter Grünberg Institute (PGI-6), Leo-Brandt-Straβe, 52428 Jülich, Germany
[h] Duisburg-Essen University, Department of Physics and Center for Nanointegration Duisburg-Essen (CENIDE), 47048 Duisburg, Germany
[i] CNR – IOM, Lab. TASC, Basovizza S.S. 14, km 163.5, 34149 Trieste, Italy

† Electronic supplementary information (ESI) available: Optimized coordinates of the free D_{4h} NiTPP; schematic representation of the free D_{4h} NiTPP; schematic representation of $^{nn}Cu^{S}_{ffh}$ 4s AOs SALC of symmetry *a*, *b* and *e*; schematic representation of the $^{nnn}Cu^{S}_{ffh}$ 4s AOs SALC of symmetry *a*, *b* and *e*. See DOI: https://doi.org/10.1039/d3cp04021f

Open Access Article. Published on 13 September 2023. Downloaded on 3/3/2026 10:42:57 PM.
This article is licensed under a Creative Commons Attribution-NonCommercial 3.0 Unported Licence.

and the additional ligands increases the M coordination number, and usually reduces the magnetic anisotropy because of the symmetry reduction of the M environment, which lowers the energy barrier among different magnetic configurations. It is also noteworthy that electronic and structural factors including the occupation number of M-based 3d atomic orbitals (AOs), the M oxidation number, and the complex conformational flexibility,[26–29] influence reactivity towards axial ligands.

Among the numerous M-porphyrin/metal interfaces studied so far,[13] the NiTPP/Cu(100) interface (the free NiTPP corresponds to Ni(II) tetraphenyl-porphyrin)[30] has received great attention because of its important role in the development of molecular materials for cutting-edge applications in spintronics, memory storage, and quantum computing.[26,31–33]

What is known so far about the NiTPP/Cu(100) interface? The experimental evidence for NiTPP/Cu(100) indicates that (i) both the adsorbate and the substrate have a local fourfold (ff) symmetry, and two NiTPP rotational domains, only slightly misaligned with respect to the Cu(100) [001] direction, are present on the surface;[31] (ii) a massive Cu(100) → NiTPP charge transfer takes place at the interface, which leads to the partial occupation of low-lying unoccupied NiTPP MOs up to LUMO+3 (LUMO stands for the lowest unoccupied MO);[31] (iii) the pristine macrocycle core (^{pmc}NiP) of the chemisorbed NiTPP has a flat geometry[32] and is characterized by the presence of the highly reactive $3d^9$ Ni(I) species.[33] Moving from experimental knowledge to the theoretical scenario, periodic density functional theory (DFT) calculations[31] indicate that the chemisorbed NiTPP assumes a bowl-shaped arrangement,[34] whose base corresponds to the ^{pmc}NiP core, which maintains its planarity and lies ∼2 Å above the Cu(100) surface. In addition, the numerical experiments carried out by Zamborlini *et al.*[31] confirm the substantial substrate → NiTPP charge transfer implying the partial occupation of the low-lying NiTPP virtual orbitals. Therefore, numerical experiments carried out with the Amsterdam density functional (ADF)[35] package on free D_{4h} CuTPP (isoelectronic with the chemisorbed NiTPP typical for the presence of the $3d^9$ Ni(I) species) indicate that the empty, low-lying, highly delocalized ^{pmc}CuP-based π orbitals ($^{pmc}\pi^*$) are the doubly degenerate $13e_g$ and the $9b_{1u}$ MOs, while the half-occupied $^{pmc}\sigma^*$ orbital, accounting for the antibonding Cu–N σ interaction and strongly localized on the $3d^9$ Cu(II) $3d_{x^2-y^2}$ AO, corresponds to the $12b_{1g}$ MO.[36] All these data lead us to assume that the experimentally revealed Cu(100) → NiTPP massive charge transfer up to LUMO+3 involves, besides the empty Ni(II)-based $12b_{1g}$ $^{pmc}\sigma^*$ LUMO+2, the whole set of low-lying $^{pmc}\pi^*$ MOs (LUMO, LUMO+1, and LUMO+3).[37]

Despite such a huge amount of electronic and structural information, a precise understanding, at the molecular level, of the Cu(100) → NiTPP charge transfer is still lacking. As a matter of fact, neither the recognition of the adsorbate and substrate MOs involved in such a process nor the identification of the Cu surface atoms (Cu^S) involved in the partial filling of the low-lying NiTPP virtual orbitals is unambiguously reported in the literature. In this paper, elementary symmetry and geometry arguments were used in combination with experimental literature reports and novel structural photoelectron diffraction (PED) results to provide a convincing molecular picture of NiTPP grafting to the substrate and then a local point of view of the Cu(100) → NiTPP charge transfer. Moreover, it is shown that the experimentally reported Ni(II) → Ni(I) reduction at the interface[33] provides the fingerprint of the chemisorption site of the NiTPP on Cu(100).

Experimental and computational details

PED experiments have been performed at the ALOISA beamline of the Elettra synchrotron radiation facility in Trieste[38] and in an ultra-high vacuum (UHV) experimental chamber with a base pressure of 10–11 mbar. Measurements have been accomplished with photon energies ranging from 850 to 1440 eV and the intensity of the Ni 2p core level was monitored with the detector (acceptance angle of 2°, FWHM) aligned along the surface normal and the surface oriented at 4° grazing angle (in close to p-polarization). Prior to the intensity integration of the Ni 2p lines, a Shirley-like background has been subtracted from each spectrum. Then, the intensity modulation curve as a function of the kinetic energy of the photoelectron has been normalized to the photon flux and the calculated Ni 2p cross-section in the measured photon energy range.[39] Reference high-resolution X-ray photoelectron spectroscopy (XPS) spectra of the N and C 1s regions have been collected at a photon energy of 515 eV by using linearly p-polarized light at a grazing incidence of 4° on the sample surface and by maintaining the hemispherical electron energy analyzer in the normal emission geometry. The binding energies in the XPS data have been referred to the Fermi level of the Cu(100) substrate. The clean Cu(100) surface has been prepared by cycles of Ar^+ ion sputtering at 2.0 keV, followed by annealing at 800 K. The absence of contaminants on the surface has been verified by XPS measurements at 650 eV (O 1s) and 515 eV (N and C 1s). The ordering of the surface and the molecular layer has been performed using the reflective high-energy electron diffraction technique. A few dozen mg of NiTPP powder (Porphyrin Systems) have been loaded in a quartz crucible of a homemade Knudsen cell-type evaporator. Before the measurements, the NiTPP sample has been carefully degassed at 480 K for several days while the base pressure of the UHV system was monitored. NiTPP molecules have been then thermally evaporated at ∼550 K onto the copper substrate maintained at room temperature. The molecular coverage has been calibrated with a quartz micro-balance, and the resulting deposition rate was 15 min ML^{-1}. The nominal coverage for all experiments herein presented is a saturated monolayer. Therefore, it is well known that organic molecules tend to decompose when exposed to ionizing radiation. XPS spectra have been then monitored over time to exclude any possible radiation-induced damage. No spectral changes were observed after 1 h, so we confirm that NiTPP molecules are reasonably stable under the adopted experimental conditions.

 This journal is © the Owner Societies 2023

Open Access Article. Published on 13 September 2023. Downloaded on 3/3/2026 10:42:57 PM.
This article is licensed under a Creative Commons Attribution-NonCommercial 3.0 Unported Licence.

The ground state electronic and structural properties of the free NiTPP are herein investigated by using the ADF package[35] within the assumption of an idealized D_{4h} symmetry[40] (see Fig. S1 in the ESI†) and by performing nonrelativistic DFT calculations whose set up (generalized gradient corrections self-consistently included through the Becke–Perdew formula,[41,42] a triple-ζ with a polarization function Slater-type basis set for all the atoms, Ni 1s–2p AOs and N and C 1s AO kept frozen throughout the calculations) has been provided by the possibility of comparing the results of our calculations with homogeneous theoretical outcomes pertinent to the free CuTPP.[36]

Results and discussion

Chemically selected quantitative structural information about the local adsorption geometry of NiTPP on Cu(100) can be obtained by monitoring the intensity of the Ni 2p core level line as a function of the energy of the incoming photon. In the PED process, the photoelectron can undergo a series of scattering processes from the scatter atoms (Cu) surrounding the emitter (Ni) along its path to the detector. The final state results from the interference between the direct and the coherently scattered components of the photoelectron signal. Thus, the resulting interference is determined by the path-length differences and the scattering phase shifts between the electron waves. These in turn depend on the kinetic energy of the electron, the detector geometry, and the position of the emitter atom relative to the scatters. By varying the kinetic energy of the emitted electrons, the interference conditions can be changed, and the modulations of the photoemission intensity may be used to extract geometrical information, which allows determination of the position of the Ni atom with respect to the copper substrate. As already mentioned, the oscillations of the core level line intensity as a function of the wave vector k of the outgoing electron ($I(k)$) contain information relative to the diffraction processes at the interface. The scattering anisotropy $\chi(k)$ can be described by eqn (1):

$$\chi(k) = \frac{I(k)}{I_{avg}} - 1 \quad (1)$$

where $I(k)$ is the measured intensity and I_{avg} is the average one.

Numerical simulations of PED data have been carried out using the MSCD package[43] (multiple scattering up to the eighth order and a Rehr–Albers order[44] of 2 have been used) and by considering three diverse chemisorption sites (atop, bridge, and ff hollow) shown schematically in Fig. 1. The obtained results have been then tested by means of the usually adopted reliability factor R_f (see eqn (2)):

$$R_f = \frac{\sum(\chi_{exp} - \chi_{th})^2}{\sum(\chi_{exp}{}^2 - \chi_{th}{}^2)} \quad (2)$$

where χ_{exp} and χ_{th} correspond to the experimental and the simulated anisotropies, respectively (see Fig. 2).

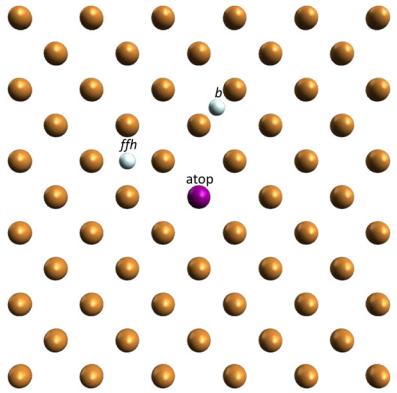

Fig. 1 Schematic representation of the atop, bridge (b), and ff hollow (ffh) chemisorption sites on the bulk terminated Cu(100) topmost layer.

R_f corresponding to the Ni species placed on an ff hollow site (R_f^{ffh}) has, among the diverse chemisorption positions herein considered, the minimum value ($R_f^{ffh} \sim 0.54$, $R_f^{atop} \sim 0.7$, and $R_f^{bridge} \sim 0.84$; see Fig. 3). In addition, the analysis of the PED data provides the following structural information: the adsorption height of Ni from the outermost layer of the substrate and the internuclear distance between Ni and the nearest-neighbors

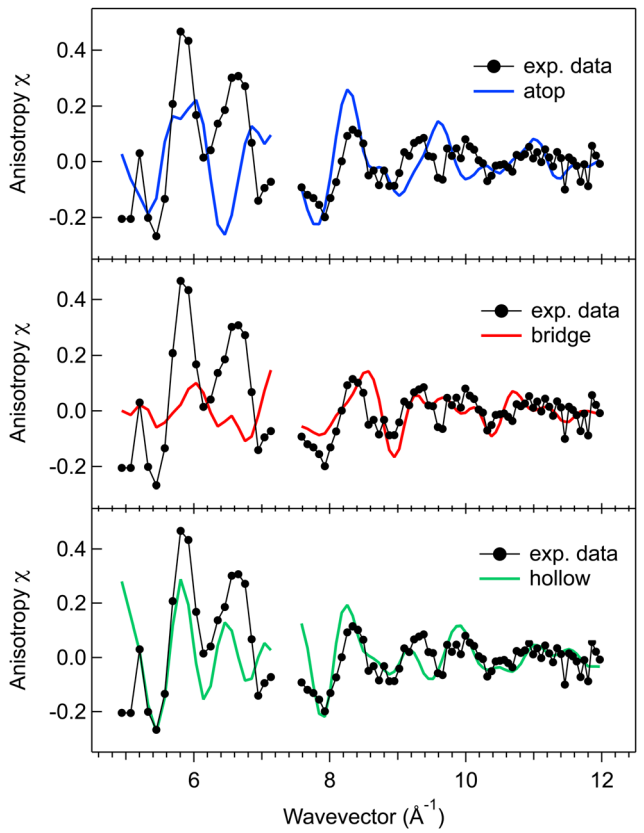

Fig. 2 PED anisotropy χ measured with the detector along the surface normal for the Ni 2p core level. The corresponding simulation, which includes a coarse optimization of the inner potential (namely 10 eV), performed for the Ni atom placed at the atop (top), bridge (middle), and ff hollow (bottom) sites are superimposed on the spectrum.

Open Access Article. Published on 13 September 2023. Downloaded on 3/3/2026 10:42:57 PM.
This article is licensed under a Creative Commons Attribution-NonCommercial 3.0 Unported Licence.

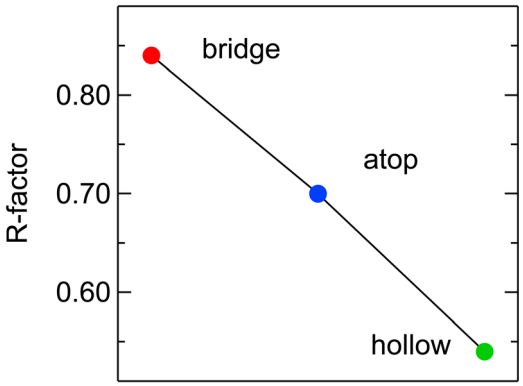

Fig. 3 Calculated R-factor (R_f) for the three different adsorption sites herein considered.

of the substrate ($^{nn}Cu^S$) are 1.95/2.66, 2.6/2.6, and 2.5/2.8 Å at the ffh, atop, and bridge chemisorption sites, respectively.

The most favored ffh site has been further refined by varying the height of Ni from the substrate and the inner potential (V_0). The resulting best fit provides the following values: $R_f^{ffh} = 0.52$, a Ni–Cu^S height of 1.93 Å, and $V_0 = 10.7$ eV (see the corresponding map in Fig. 4).

PED measurements at normal emission are best suited for determining the vertical distance of the emitter from the surface and the structural information herein obtained perfectly agrees with experimental and theoretical literature data pertaining not only to the NiTPP/Cu(100) system,[31] but also to similar MTPP adsorbed on Cu(111) and Cu(110) surfaces.[45,46] Nevertheless, we cannot be silent about the aptitude, substantially phenomenological, characterizing all this matter. In other words, neither experimental nor theoretical literature results provide an answer to the question of why the ffh chemisorption site of the NiTPP/Cu(100) interface is more stable than those on the atop and bridge ones. Let us see how the exploitation of elementary symmetry considerations allows us to gain further insights into this issue.

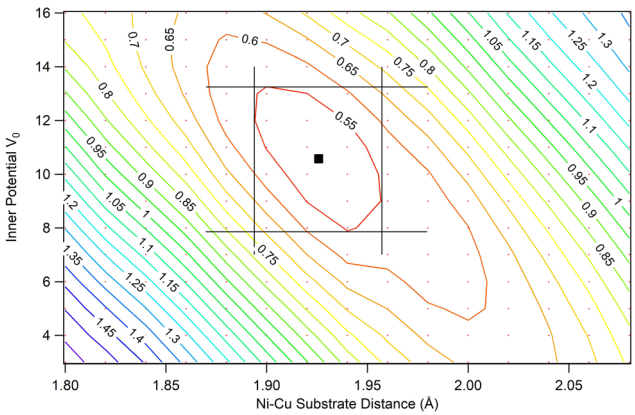

Fig. 4 Contour plot of the MSCD simulation R_f^{ffh} for the inner potential V_0 and the Ni–Cu substrate distance. Black lines correspond to the region where R_f^{ffh} is $\leq$ 0.55 and the lowest R_f^{ffh} = 0.52 corresponds to a Ni–Cu substrate distance of 1.93 Å and V_0 = 10.7 eV.

The ff quantization axis, characteristic of the free NiTPP (see Fig. S1 in the ESI†), lifts the fivefold degeneracy of the Ni(II) 3d AOs to generate five MOs transforming as the a (z^2), b ($x^2 - y^2$ and xy), and e (xz, yz) irreducible representations (IRs) of the C_4 point group.[40] All of these MOs, except the $^{pmc}\sigma^*$ one, are fulfilled; hence, only the $3d_{x^2-y^2}$ AO of the pristine $3d^8$ Ni(II) can accept charge regardless of the NiTPP chemisorption site. Upon NiTPP deposition on Cu(100), the N-chelated Ni species is effectively reduced to the oxidation state +1 thus assuming a $3d^9$ configuration, as measured by X-ray absorption spectroscopy at the Ni L_3-edge.[33] Since the ff quantization axis is locally preserved in the adsorbate as well as in the substrate,[31] we can assess that: (i) a single Cu^S atom lying on the ff axis may transfer electronic charge only through its half-occupied 4s AO (of symmetry a in the C_4 point group),[40] and (ii) the symmetry adapted linear combinations (SALC) of 4s AOs localized on four equivalent Cu^S atoms transform as $a + b + e$ IRs of the C_4 point group.[40]

These elementary symmetry considerations exclude the possibility that the Ni(II) → Ni(I) reduction is driven by a charge transfer from a Cu^S atom beneath Ni when NiTPP is chemisorbed on Cu(100) atop a ff surface atom (Cu^s_{ffa}). More specifically, the single $^{nn}Cu^s_{ffa}$ located at 2.6 Å from Ni (see above) could transfer electronic charge to Ni(II) only through its half-occupied 4s AO, which transforms as the IR a of the C_4 group. This AO is orthogonal to the empty MO localized on the Ni atom (namely, on Ni(II) $3d_{x^2-y^2}$ AO, transforming as the IR b of the C_4 group[40]) reminiscent of the NiTPP $^{pmc}\sigma^*$ $12b_{1g}$ LUMO+2 (see Fig. 5),[47] and then the transfer is symmetry forbidden.

Before applying analogous symmetry arguments to the chemisorption of NiTPP at a Cu(100) ffh site,[48] it deserves to be noticed that the internuclear distance between Ni and each of the four $^{nnn}Cu^s_{ffa}$ (nnn stands for next nearest neighbor) in the bulk terminated Cu(100) surface amounts to 3.646 Å;[49] too far to have an effective overlap between the empty $^{pmc}\sigma^*$ $12b_{1g}$ MO and the SALC of symmetry b of the $^{nnn}Cu^s_{ffa}$ 4s AOs shown in Fig. 6.

Examination of Fig. 7 clearly shows that the ffh chemisorption site is much more suitable to foster the Ni(II) → Ni(I) reduction.

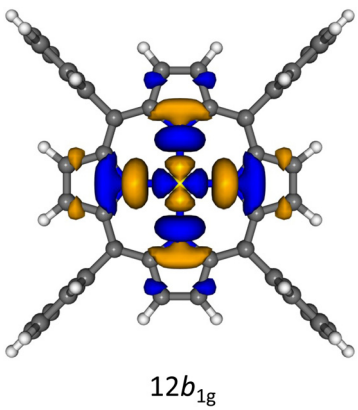

Fig. 5 3D contour plot (CP) of the free D_{4h} NiTPP $^{pmc}\sigma^*$ $12b_{1g}$ LUMO+2.[47] Displayed isosurfaces correspond to ± 0.02 $e^{1/2} \times Å^{-3/2}$ values. The ^{pmc}NiP core lies in the xy plane in the adopted framework.

Open Access Article. Published on 13 September 2023. Downloaded on 3/3/2026 10:42:57 PM.
This article is licensed under a Creative Commons Attribution-NonCommercial 3.0 Unported Licence.

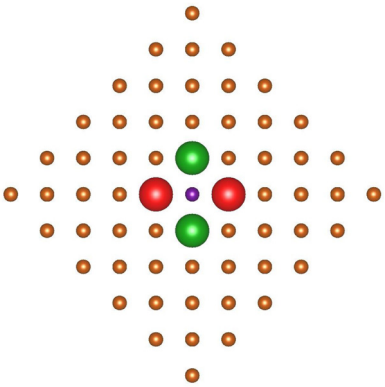

Fig. 6 Schematic representation of the $^{nnn}Cu^{S}_{ffa}$ 4s AOs SALC of symmetry *b*. Large red and green spheres represent Cu^{S} 4s AOs and corresponding different phases.

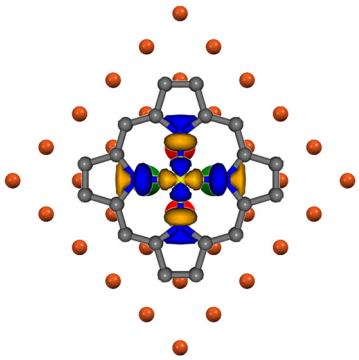

Fig. 8 Superposition of the $^{pmc}\sigma^{*}$ $12b_{1g}$-based MO (LUMO+2)[37] 3D CP to the $^{nn}Cu^{S}_{ffh}$ 4s AOs SALC of symmetry *b* of the bulk terminated Cu(100). Ni–N bonds are aligned with the ⟨001⟩ directions. Large red and green spheres represent Cu^{S} 4s AOs and corresponding different phases.

In fact, (i) at the ffh chemisorption site, the internuclear distance between Ni and its four nearest neighbors ($^{nn}Cu^{S}_{ffh}$) is 2.644 Å;[50] (ii) the SALC of symmetry *b* of the $^{nn}Cu^{S}_{ffh}$ 4s AOs (see Fig. S2 in the ESI†) perfectly overlaps with the empty Ni(II)-based $^{pmc}\sigma^{*}$ MO when the Ni–N bonds are aligned with the ⟨001⟩ directions (see the right panel of Fig. 7 and 8); (iii) periodic DFT calculations carried out by some of us[31] ultimately indicated that, among the atop, bridge, and ffh chemisorption sites, the ffh one is more stable than the atop and bridge sites by 2 and 1 eV, respectively. Therefore, it is noteworthy that the higher stability of the ffh site for NiTPP on Cu(100) agrees well with the experimental evidence pertaining to M(II) phthalocyanine (Fe, Co, Cu, and Zn) deposited on the same substrate:[51–54] a fulfilled M $3d_{z^2}$ AO (M = Cu and Zn) favours the ffh site,[53,54] while a partially occupied M $3d_{z^2}$ AO (M = Fe and Co) fosters the ffa one.[51,52] This is not surprising if we consider that, at the ffa site, the antibonding combination of the M $3d_{z^2}$ and $^{nn}Cu^{S}_{ffh}$ 4s AOs (both of them transforming as the IR *a* of the C_4 point group)[40] would be populated (vacant) if the M $3d_{z^2}$ AO is fulfilled (half-filled).

Besides a rationale for the experimentally reported Ni(II) → Ni(I) reduction,[33] a real fingerprint of the NiTPP chemisorption site on Cu(100), the same simple arguments can be used to gain insights into the substrate → adsorbate charge transfer involving the doubly degenerate $^{pmc}\pi^{*}$ orbitals reminiscent of the NiTPP $13e_g$ LUMO (see the left panel in Fig. 9). Examination of the figure reveals that the $13e_g$-based MOs, significantly localized on the N $2p_{\pi}$ AOs of the ^{pmc}NiP core, can constructively overlap with the $^{nn}Cu^{S}_{ffh}$ 4s AOs SALC of symmetry *e* of the bulk terminated Cu(100) (see Fig. S2 in the ESI† and the right panel of Fig. 9).

As such, it is noteworthy that the $^{nn}Cu^{S}_{ffh}$–N distance with the ^{pmc}NiP core of the optimized D_{4h} NiTPP at 1.93 Å from the bulk terminated Cu(100) surface and the Ni–N bonds aligned with the ⟨001⟩ directions is, as pointed out by Zamborlini *et al.*,[31] "extremely short" (1.938 Å in the model herein considered).[55]

Angle-resolved photoemission tomography experiments at the NiTPP/Cu(100) interface revealed that the massive substrate → adsorbate charge transfer takes place through the partial filling of ^{pmc}NiP low-lying unoccupied MOs up to LUMO+3.[31] The last one is reminiscent of the D_{4h} NiTPP $^{pmc}\pi^{*}$ $9b_{1u}$ MO, which, for symmetry reasons,[56] bears no density of states on the

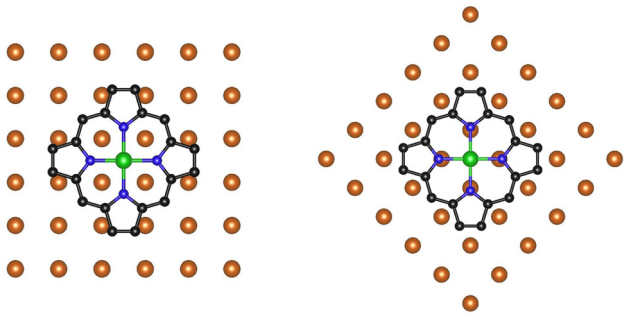

Fig. 7 Schematic representation of the ^{pmc}NiP core superimposed to the bulk terminated Cu(100) at a ffh site. Only atoms of the Cu(100) topmost layer are displayed and the planar ^{pmc}NiP core[31] of the optimized free D_{4h} NiTPP is placed 1.93 Å above it. In the left (right) panel, the Ni–N bonds are aligned with the ⟨011⟩ (⟨001⟩) directions.

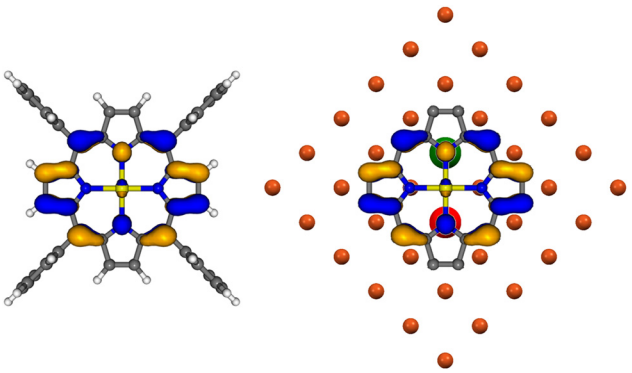

Fig. 9 (left panel) 3D CP of one component of the free D_{4h} NiTPP $^{pmc}\pi^{*}$ $13e_g$ LUMO;[37] (right panel) superposition of the same component of the doubly degenerate $^{pmc}\pi^{*}$ $13e_g$-based MO to the $^{nn}Cu^{S}_{ffh}$ 4s AOs SALC of symmetry *e* of the bulk terminated Cu(100). Ni–N bonds are aligned with the ⟨001⟩ directions. Large red and green spheres represent Cu^{S} 4s AOs and corresponding different phases.

Open Access Article. Published on 13 September 2023. Downloaded on 3/3/2026 10:42:57 PM.
This article is licensed under a Creative Commons Attribution-NonCommercial 3.0 Unported Licence.

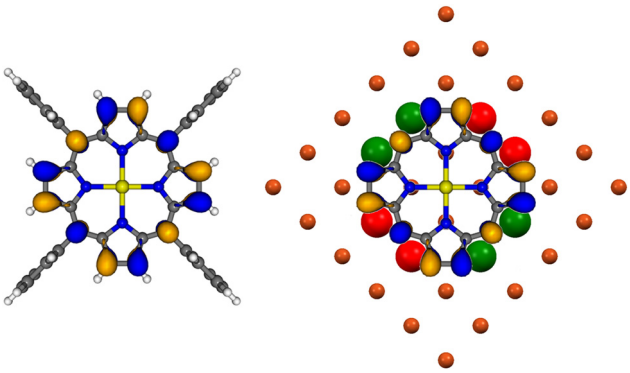

Fig. 10 (left panel) 3D CP of the free D_{4h} NiTPP $^{pmc}\pi^*$ $9b_{1u}$ MO (LUMO+3); (right panel) superposition of the same $^{pmc}\pi^*$ MO to the $^{nnn}Cu^{S}_{ffh}$ 4s AOs SALC of symmetry *b* of the bulk terminated Cu(100). Ni–N bonds are aligned with the ⟨001⟩ directions. Large red and green spheres represent Cu^{S} 4s AOs and corresponding different phases.

N atoms; hence, its nodal properties prevent any possibility to receive charge from the $^{nn}Cu^{S}_{ffh}$ 4s AOs SALC of symmetry *b* (see Fig. S2 of the ESI†), while the opposite is true when the eight $^{nnn}Cu^{S}_{ffh}$ are considered. The SALCs of the $^{nnn}Cu^{S}_{ffh}$ 4s AOs transform as $2a + 2b + 2e$ and are sketched in Fig. S3 of the ESI.† Inspection of this figure reveals that the nodal properties of the SALC labeled 2*b* in Fig. S3 (ESI†) make it very well suited for transferring electronic charge into the $^{pmc}\pi^*$ $9b_{1u}$-like MO (see Fig. 10).

Analogous considerations hold for the $^{nnn}Cu^{S}_{ffh}$ SALCs labeled 1*e* in Fig. S3 in the ESI,† which may contribute to the Cu(100) → ^{pmc}NiP charge transfer by involving the C^{meso} $2p_{\pi}$ AOs (see Fig. 11) of the $^{pmc}\pi^*$ $13e_g$-based MOs (LUMO/LUMO+1).

As such, it can be useful to mention that, with the ^{pmc}NiP core of the optimized D_{4h} NiTPP at 1.93 Å from the surface, and the highly reactive species Ni(I) located at the ffh site, the internuclear distances of the eight $^{nnn}Cu^{S}_{ffh}$ from the ^{pmc}NiP α and β pyrrolic C atoms are 2.204 and 2.311 Å, respectively, while the internuclear distance between $^{nnn}Cu^{S}_{ffh}$ and C^{meso} atoms is 2.348 Å.[57]

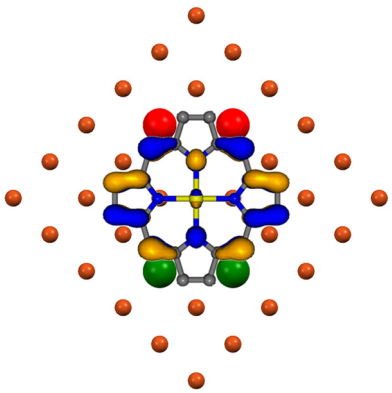

Fig. 11 Superposition of one component of the doubly degenerate $^{pmc}\pi^*$ $13e_g$-based MO to the $^{nnn}Cu^{S}_{ffh}$ 4s AOs SALC of symmetry *e* of the bulk terminated Cu(100). Ni–N bonds are aligned with the ⟨001⟩ directions. Large red and green spheres represent Cu^{S} 4s AOs and corresponding different phases.

Conclusions

The experimentally reported Ni(II) → Ni(I) reduction of NiTPP/Cu(100) controls the molecular adsorption at an ffh site, as well as the alignment of the Ni–N bonds along the substrate ⟨001⟩ directions. Therefore, the Ni reduction is driven by the charge transfer into the Ni $3d_{x^2-y^2}$-based $12b_{1g}$ MO (LUMO+2) from the four $^{nn}Cu^{S}_{ffh}$ underneath the N atoms. The same $^{nn}Cu^{S}_{ffh}$ are responsible for the charge transfer into the $^{pmc}\pi^*$ orbitals reminiscent of the NiTPP $13e_g$ LUMO/LUMO+1 strongly localized on the N atoms, whereas the partial filling of the $^{pmc}\pi^*$ $9b_{1u}$-based LUMO+3 (solely localized on the C atoms of the ^{pmc}NiP core) is driven by the charge transfer from the eight $^{nnn}Cu^{S}_{ffh}$. The latter ones may additionally contribute to the partial filling of the LUMO/LUMO+1 through the C^{meso} atoms. In a few words, symmetry and geometry considerations herein presented provide the modeling of the NiTPP–Cu(100) anchoring configuration from an atomistic view, as dictated by the interfacial charge transfer.

Author contributions

We strongly encourage authors to include author contributions and recommend using CRediT for standardised contribution descriptions. Please refer to our general author guidelines for more information about authorship.

Conflicts of interest

There are no conflicts to declare.

Notes and references

1 A. Ghosh, *Letters to a young Chemist*, JohnWiley & Sons, Hoboken, NJ, USA, 2011; p. 34.
2 D. L. Nelson, M. M. Cox and A. A. Hoskins, *Lehninger Principles of Biochemistry*, Freeman, W.H. Macmillan learning, New York, NY, USA, 8th edn, 2021.
3 J. M. Berg, J. L. Tymoczko and L. Stryer, *Biochemistry*, W. H. Freeman, New York, NY, USA, 5th edn, 2002.
4 A. R. Battersby, C. J. R. Fookes, G. W. J. Matcham and E. McDonald, *Nature*, 1980, **285**, 17–21.
5 A. R. Battersby, *Nat. Prod. Rep.*, 1987, **4**, 77–87.
6 X. Xue, A. Lindstrom and Y. Li, *Bioconjugate Chem.*, 2019, **30**, 1585–1603.
7 A. Tsuda and A. Osuka, *Science*, 2001, **293**, 79–82.
8 M. Planells, A. Forneli, E. Martínez-Ferrero, A. Sánchez-Díaz, M. A. Sarmentero, P. Ballester, E. Palomares and B. C. O'Regan, *Appl. Phys. Lett.*, 2008, **92**, 153506.
9 N. A. Rakow and K. S. Suslick, *Nature*, 2000, **406**, 710–713.
10 *The Porphyrin Handbook*, ed. K. M. Kadish, K. M. Smith and R. Guilard, Academic Press, New York, NY, USA, 2000.
11 D. Dini and M. Hanack, *J. Porphyrins Phthalocyanines*, 2004, **8**, 915–933.
12 C. Di Natale, D. Monti and R. Paolesse, *Mater. Today*, 2010, **13**, 46–52.

Open Access Article. Published on 13 September 2023. Downloaded on 3/3/2026 10:42:57 PM.
This article is licensed under a Creative Commons Attribution-NonCommercial 3.0 Unported Licence.

13 J. M. Gottfried, *Surf. Sci. Rep.*, 2015, **70**, 259–379.
14 C. M. Drain, *Proc. Natl. Acad. Sci. U. S. A.*, 2002, **99**, 5178–5182.
15 G. L. Miessler, P. J. Fischer and D. A. Tarr, *Inorganic Chemistry*, Pearson, New York, NY, USA, 5th edn, 2013, p. 137.
16 M. Dyer, A. Robin, S. Haq, R. Raval, M. Persson and J. Klime, *ACS Nano*, 2011, **5**, 1831–1838.
17 F. Bischoff, K. Seufert, W. Auwärter, S. Joshi, S. Vijayaraghavan, D. Écija, K. Diller, A. C. Papageorgiou, S. Fischer, F. Allegretti, D. A. Duncan, F. Klappenberger, F. Blobner, R. Han and J. V. Barth, *ACS Nano*, 2013, **7**, 3139–3149.
18 H. Wende, M. Bernien, J. Luo, C. Sorg, N. Ponpandian, J. Kurde, J. Miguel, M. Piantek, X. Xu, P. Eckhold, W. Kuch, K. Baberschke, P. M. Panchmatia, B. Sanyal, P. M. Oppeneer and O. Eriksson, *Nat. Mater.*, 2007, **6**, 516–520.
19 C. Wäckerlin, D. Chylareck, A. Kleibert, K. Müller, C. Iacovita, F. Nolting, T. A. Jumg and N. Ballav, *Nat. Commun.*, 2010, **61**, 1–7.
20 S. Lach, A. Altenhof, K. Tarafder, F. Schmitt, M. E. Ali, M. Vogel, J. Sauther, P. M. Oppeneer and C. Ziegler, *Adv. Funct. Mater.*, 2012, **22**, 989–997.
21 S. Jakobs, A. Narayan, B. Stadtmüller, A. Droghetti, I. Rungger, Y. S. Hor, S. Klyatskaya, D. Jungkenn, J. Stöckl, M. Laux, O. L. A. Monti, M. Aeschlimann, R. J. Cava, M. Ruben, S. Mathias, S. Sanvito and M. Cinchetti, *Nano Lett.*, 2015, **15**, 6022–6029.
22 P. Gambardella, S. Stepanow, A. Dmitriev, J. Honolka, F. M. F. De Groot, M. Lingenfelder, S. Sen Gupta, D. D. Sarma, P. Bencok, S. Stanescu, S. Clair, S. Pons, N. Lin, A. P. Seitsonen, H. Brune, J. V. Barth and K. Kern, *Nat. Mater.*, 2009, **8**, 189–193.
23 C. Wäckerlin, K. Tarafder, J. Girovsky, J. Nowakowski, T. Hählen, A. Shchyrba, D. Siewert, A. Kleibert, F. Nolting, P. M. Oppeneer, T. A. Jung and N. Ballav, *Angew. Chem., Int. Ed.*, 2013, **52**, 4568–4571.
24 J. Miguel, C. F. Hermanns, M. Bernien, A. Krüger and W. Kuch, *J. Phys. Chem. Lett.*, 2011, **2**, 1455–1459.
25 I. Cojocariu, S. Carlotto, H. M. Sturmeit, G. Zamborlini, M. Cinchetti, A. Cossaro, A. Verdini, L. Floreano, M. Jugovac, P. Puschnig, C. Piamonteze, M. Casarin, V. Feyer and C. M. Schneider, *Chem. – Eur. J.*, 2021, **27**, 3526–3535.
26 H. M. Sturmeit, I. Cojocariu, A. Windischbacher, P. Puschnig, C. Piamonteze, M. Jugovac, A. Sala, C. Africh, G. Comelli, A. Cossaro, A. Verdini, L. Floreano, M. Stredansky, E. Vesselli, C. Hohner, M. Kettner, J. Libuda, C. M. Schneider, G. Zamborlini, M. Cinchetti and V. Feyer, *Small*, 2021, **17**, 2104779.
27 I. Cojocariu, S. Carlotto, G. Zamborlini, M. Jugovac, L. Schio, L. Floreano, M. Casarin, V. Feyer and C. M. Schneider, *J. Mater. Chem. C*, 2021, **9**, 12559–12565.
28 I. Cojocariu, S. Carlotto, N. Jugovac, L. Floreano, M. Casarin, V. Feyer and C. M. Schneider, *J. Mater. Chem. C*, 2022, **10**, 9748–9757.
29 P. Knecht, J. Reichert, P. S. Deimel, P. Feulner, F. Haag, F. Allegretti, M. Garnica, M. Schwarz, W. Auwärter, P. T. P. Ryan, T. L. Lee, D. A. Duncan, A. P. Seitsonen, J. V. Barth and A. C. Papageorgiou, *Angew. Chem., Int. Ed.*, 2021, **60**, 16561–16567.
30 Optimized Cartesian coordinates of the free D_{4h} NiTPP are reported in Table S1 of the ESI while its structure is displayed in Fig. S1 of the ESI†.
31 G. Zamborlini, D. Lüftner, Z. Feng, B. Kollmann, P. Puschnig, C. Dri, M. Panighel, G. Di Santo, A. Goldoni, G. Comelli, M. Jugovac, V. Feyer and C. M. Schneider, *Nat. Commun.*, 2017, **8**, 1–8.
32 I. Cojocariu, H. M. Sturmeitb, G. Zamborlini, A. Cossaro, A. Verdini, L. Floreano, E. D'Incecco, M. Stredansky, E. Vesselli, M. Jugovaca, M. Cinchetti, V. Feyer and C. M. Schneider, *Appl. Surf. Sci.*, 2020, **504**, 144343.
33 G. Zamborlini, M. Jugovac, A. Cossaro, A. Verdini, L. Floreano, D. Lüftner, P. Puschnig, V. Feyer and C. M. Schneider, *Chem. Commun.*, 2018, **54**, 13423–13426.
34 The NiTPP Ph rings bonded to C^m are upwards tilted. The tilt angle ϕ, defined as the angle between the ^{pcm}NiP plane and the C–C bond connecting Ph rings to C^m atoms, amounts to $\sim 140^\circ$ (see Fig. 2d of ref. 31).
35 ADF2014, SCM, Theoretical Chemistry, Vrije Universiteit, Amsterdam, The Netherlands, **https://www.scm.com**.
36 G. Mangione, M. Sambi, S. Carlotto, A. Vittadini, G. Ligorio, M. Timpel, L. Pasquali, A. Giglia, M. V. Nardi and M. Casarin, *Phys. Chem. Chem. Phys.*, 2016, **18**, 24890–24904.
37 To avoid any ambiguity, it must be kept in mind that the free D_{4h} NiTPP LUMO and LUMO+1 correspond to the two components of the degenerate $13e_g$ orbital.
38 L. Floreano, G. Naletto, D. Cvetko, R. Gotter, M. Malvezzi, L. Marassi, A. Morgante, A. Santaniello, A. Verdini, F. Tommasini and G. Tondello, *Rev. Sci. Instrum.*, 1999, **70**, 3855–3864.
39 (*a*) J. J. Yeh, *Atomic calculation of photoionization cross-sections and asymmetry parameters*, Gordon and Breach, Langhorne, PA, USA, 1993; (*b*) J. J. Yeh and I. Lindau, Atomic Subshell Photoionization Cross Section and Asymmetry Parameters: $1 \leq Z \leq 103$, *At. Data Nucl. Data Tables*, 1985, **32**, 1–155.
40 B. E. Douglas and C. A. Hollingsworth, *Symmetry in Bonding and Spectra, an Introduction*, Academic Press, Orlando, FL, USA, 1985.
41 A. D. Becke, *Phys. Rev. A: At., Mol., Opt. Phys.*, 1988, **38**, 3098–3100.
42 J. P. Perdew, *Phys. Rev. B: Condens. Matter Mater. Phys.*, 1986, **33**, 8822–8824.
43 Y. Chen, F. J. García de Abajo, A. Chassé, R. X. Ynzunza, A. P. Kaduwela, M. A. Van Hove and C. S. Fadley, *Phys. Rev. B: Condens. Matter Mater. Phys.*, 1998, **58**, 13121–13131.
44 J. J. Rehr, R. C. Albers and S. I. Zabinsky, High-Order Multiple-Scattering Calculations of X-Ray-Absorption Fine Structure, *Phys. Rev. Lett.*, 1992, **69**, 3397–3400.
45 M. Schwarz, M. Garnica, D. A. Duncan, A. P. Paz, J. Ducke, P. S. Deimel, P. K. Thakur, T.-L. Lee, A. Rubio, J. V. Barth, F. Allegretti and W. Auwärter, *J. Phys. Chem. C*, 2018, **122**, 5452–5461.

Open Access Article. Published on 13 September 2023. Downloaded on 3/3/2026 10:42:57 PM.
This article is licensed under a Creative Commons Attribution-NonCommercial 3.0 Unported Licence.

46 P. Donovan, A. Robin, M. S. Dyer, M. Persson and R. Raval, *Chem. – Eur. J.*, 2010, **16**, 11641–11652.

47 The empty $^{pmc}\sigma^*$ $12b_{1g}$ orbital (the LUMO+2) of the free D_{4h} NiTPP is undistinguishable both in shape and localization from the half-occupied CuTPP $12b_{1g}$ MO.[36] 3D CPs have been obtained by using the open-source multi-platform molecular visualization program Molekel 5.4.

48 At the bridge chemisorption site, the local twofold symmetry (see Fig. 1) determines a very poor interaction between the $^{pmc}\sigma^*$ $12b_{1g}$-based MO and the in-phase combination of the two 4s AOs localized on the two $^{nn}Cu^S$, whose internuclear distance from Ni is 2.8 Å. This is why the bridge site will not be taken into consideration further.

49 The $^{nnn}Cu_{ffa}{}^S$–Ni distance of 3.646 Å is obtained by using the Ni–Cu^S height of 2.6 Å and a Cu cell parameter of 3.6149 Å https://(https://www.webelements.com/).

50 The $^{nn}Cu_{ffh}{}^S$–Ni distance of 2.644 Å is obtained by using the Ni–Cu^S height of 1.93 Å and a Cu cell parameter of 3.6149 Å https://(https://www.webelements.com/).

51 Q. Guo, Z. Qin, K. Zang, C. Liu, Y. Yu and G. Cao, *Langmuir*, 2010, **26**, 11804–11808.

52 P. H. Lippel, R. J. Wilson, M. D. Miller, Ch Wöll and S. Chiang, *Phys. Rev. Lett.*, 1989, **62**, 171–174.

53 H. Okuyama, S. Kuwayama, Y. Nakazawa, S. Hatta and T. Aruga, *Surf. Sci.*, 2022, **723**, 1–7.

54 F. Chen, X. Chen, L. Liu, X. Song, S. Liu, J. Liu, H. Ouyang, Y. Cai, X. Liu, H. Pan, J. Zhu and L. Wang, *Appl. Phys. Lett.*, 2012, **100**, 081602.

55 The $^{nn}Cu_{ffh}{}^S$–N distance of 1.938 Å is obtained by using the Ni–Cu^S height of 1.93 Å, the herein optimized Ni–N bond length of 1.980 Å and a Cu cell parameter of 3.6149 Å https://(https://www.webelements.com/).

56 In the free D_{4h} MTPP, with the MP pristine macrocycle plane corresponding to the *xy* one (σ_h) and the pyrrolic N atoms lying in the *xz* and *yz* planes (the two σ_v), the N $2p_z$ SALCs transform as the $e_g + a_{2u} + b_{2u}$ IRs of the D_{4h} point group.[40] The b_{1u} IR is antisymmetric with respect to σ_v[40] and then p_z AOs of atoms lying in these two planes cannot contribute to MOs of b_{1u} symmetry.

57 The ^{pmc}NiP α(β) pyrrolic C atoms correspond to C1, C4, C6, C9, C11, C14, C16, and C19 (C2, C3, C7, C8, C12, C13, C17, and C18) in Fig. S1 of the ESI†.

 This journal is © the Owner Societies 2023